FORENSIC SCIENCE JOURNAL SINCE 2002

Forensic Science Journal
2025;24(1):1-12
fsjournal.cpu.edu.tw
DOI:10.6593/FSJ.202512_24(1).0001

Mass Spectrometric Differentiation and *In Vitro* Metabolic Profiling of Fluorodeschloroketamine Positional Isomers

Ya-Ling Yeh[1,2], M.Sc.; Yu-Wei Huang[3], M.Sc.; Che-Yen Wen[1], Ph.D.; Chin-Lin Hsieh[4], Ph.D.; Sheng-Meng Wang[1*], Ph.D.

[1] Department of Forensic Science, Central Police University, Taoyuan City, Taiwan (ROC)
[2] Forensic Science Center, Taoyuan Police Department, Taoyuan City, Taiwan (ROC)
[3] Forensic Science Center, New Taipei City Police Department, New Taipei City, Taiwan (ROC)
[4] Forensic Science Center, Criminal Investigation Bureau, National Police Agency, Taipei City, Taiwan (ROC)

Received: 4 February 2025; Received in revised form 19 February 2025; Accepted 20 February 2025

Abstract

Ketamine and its analogs, such as 2-fluoro-deschloroketamine (2-FDCK), methoxetamine, deschloroketamine, and Bromodeschloroketamine, have garnered significant attention due to their widespread abuse and potential toxicity. Among these, 2-FDCK, 3-FDCK and 4-FDCK share structural similarities, yet only 2-FDCK is currently classified as a controlled substance in Taiwan. Given their differences in pharmacokinetics, pharmacodynamics, and metabolic pathways, the establishment of reliable analytical methods is crucial for forensic and toxicological investigations. In this study, we utilized Trifluoroacetic anhydride derivatization and the gas chromatography-mass spectrometry (GC-MS) to develop a mass spectral classification model for distinguishing these positional isomers. We used principal component analysis (PCA) for feature extraction and logistic regression (LR) for classification. In our experiments, the model achieved 100% accuracy in the test set. Analysis of urine samples confirmed the presence of 2-FDCK, demonstrating the method's effectiveness in differentiating *ortho*-, *meta*-, and *para*-substituted isomers. Additionally, we conducted an *in vitro* metabolism study using human liver microsomes (HLMs) and liquid chromatography-quadrupole time-of-flight mass spectrometry (LC-QTOF-MS). This analysis identified 15 metabolites, formed through hydrogenation, N-demethylation, hydroxylation, deamination, and dehydration. Among the isomers, 4-FDCK metabolized the slowest, with 48% of the parent compound remaining and dihydro-4-FDCK as the major metabolite, while 3-FDCK exhibited the fastest metabolism, with dihydro-3-FDCK as the predominant product. Comparison with urine samples confirmed nor-2-FDCK (M1), dihydro-2-FDCK (M8(a)), and dihydro-nor-2-FDCK (M9(a), M9(b)) as key biomarkers for 2-FDCK detection, particularly when the parent compound is present at low concentrations. This study establishes a mass spectral classification model and an *in vitro* metabolite database, which facilitate rapid isomer differentiation and metabolite identification. The approach provides a valuable reference for forensic and toxicological applications, aiding in the detection of structurally similar new psychoactive substances.

Keywords: forensic Science, fluorodeschloroketamine (FDCK), isomer, in vitro metabolic study, machine learning analysis

* Corresponding author: Sheng-Meng Wang, Ph.D. Department of Forensic Science, Central Police University, No.56, Shuren Rd., Guishan Dist., Taoyuan City 333322, Taiwan (ROC)
Tel: 886-3-3282321 ext 5000; Fax: 886-3-3275907
E-mail: wang531088@mail.cpu.edu.tw; jkzim13@gmail.com (Ya-Ling Yeh)

Introduction

Ketamine, a dissociative anesthetic classified as an arylcyclohexylamine, consists of three key structural components: an aryl ring, an amine group, and a cyclohexanone moiety. The aryl ring is the primary pharmacologically active site, where chlorine substitution enhances analgesic effects. The electron-rich secondary amine maintains efficacy, while the cyclohexyl group and ketone moiety influence metabolism and excretion [1]. To develop safer and more effective analogs, various ketamine derivatives have been synthesized [1]. Advances in chemical synthesis have facilitated the clandestine production of structurally modified ketamine analogs, often exhibiting comparable or greater potency [2]. Although these compounds constitute a small fraction of new psychoactive substances (NPS), they are widely abused in Asia [3]. The United Nations Office on Drugs and Crime (UNODC) classifies ketamine and its analogs under phencyclidine-type substances, which include methoxetamine (MXE), methoxpropamine (MXPr), 3-methoxyeticyclidine (3-MeO-PCE), 2-MeO-PCE, 4-MeO-PCE, 3-methoxy-phencyclidine (3-MeO-PCP), deschloro-N-ethyl-ketamine (2-oxo-PCE, O-PCE), 2-fluoro-deschloroketamine (2-FDCK), deschloroketamine (DCK) and N-ethylnorketamine [4-6]. These substances have been implicated in numerous toxicological and fatal incidents [7]. Furthermore, recreational drugs are often adulterated with other psychoactive compounds, exacerbating acute intoxication risks and complicating clinical and forensic analysis [8].

As of October 2024, 'the Substance Abuse Inspection and Notification System' of the Ministry of Health and Welfare reported the identification of 195 types of NPSs in Taiwan, including 11 ketamine and ketamine analogs, with ketamine abuse remaining a significant concern [9]. The emergence of ketamine analogs, such as 2-FDCK, MXE, DCK and Bromodeschloroketamine, highlights the need for robust analytical methods for their identification and metabolic profiling. Although 2-FDCK, 3-FDCK and 4-FDCK share structural similarities, only 2-FDCK is currently classified as a controlled substance in Taiwan. Given their positional isomerism, distinguishing these compounds is critical for forensic and toxicological investigations. Variations in pharmacokinetics and pharmacodynamics among these isomers influence absorption, distribution, metabolism, and excretion, as well as drug activity, efficacy, therapeutic applications, and toxicity profiles [10, 11]. However, differentiating *ortho*-, *meta*-, and *para*-substituted isomers remains analytically challenging. These compounds exhibit similar retention times (RT) and mass spectra in gas chromatography-mass spectrometry (GC-MS) and liquid chromatography-quadrupole time-of-flight mass spectrometry (LC-QTOF-MS), which limits conventional methods' effectiveness. To address this, several previous studies have applied chemometric techniques to isomer classification, such as principal component analysis (PCA), linear discriminant analysis (LDA), and Random Forest machine learning [12-15]. Additionally, Kranenburg et al. [16] demonstrated that propionic anhydride derivatization enhances fragmentation differences, facilitating more accurate differentiation of positional isomers.

The metabolism of 2-FDCK has been investigated using high-resolution mass spectrometry (HRMS). Mestria et al. [17] employed Orbitrap HRMS to study the metabolism of 2-FDCK in forensic blood and hair samples, identifying nor-2-FDCK, dihydro-2-FDCK, and dihydro-nor-2-FDCK as major metabolites. Similarly, Gicquel et al. [18] utilized pooled human liver microsomes (HLMs), HepaRG cells, and postmortem samples from a fatal case, identifying 17 Phase I and 3 Phase II metabolites via Orbitrap HRMS and molecular networking analysis. Their study revealed hydrogenation, N-demethylation, hydroxylation, deamination, dehydration, and glucuronidation as key metabolic pathways. Joseph et al. [2] further analyzed 2-FDCK metabolism using HLMs and applied their findings to urine, hair, and seized materials, identifying 13 metabolites in HLMs, 23 in urine, and 20 in hair. Consistent with Gicquel et al. [18], they confirmed nor-2-FDCK as the most reliable biomarker and proposed OH-dihydro-nor-2-FDCK and dehydro-nor-2-FDCK as potential alternative markers. Additionally, their study detected defluorinated metabolites (DCK) in authentic urine samples, which were absent in HLMs studies, suggesting in vivo metabolic differences.

Building upon these findings, this study aims to develop a GC-MS-based mass spectral classification model to distinguish 2-FDCK, 3-FDCK and 4-FDCK following Trifluoroacetic anhydride (TFAA) derivatization. Additionally, an *in vitro* metabolism study using LC-QTOF-MS was conducted to characterize

the metabolic profiles of these isomers, providing a metabolite database and identifying suitable detection markers. To further validate the model, four urine samples were analyzed and compared with *in vitro* metabolism results. By integrating mass spectral classification, metabolic differentiation, and real sample analysis, this study aims to improve the detection and characterization of positional isomers in NPS, addressing forensic and toxicological analytical challenges.

Materials and methods

Materials

Standards of 2-FDCK, 3-FDCK and 4-FDCK (1 mg/mL) and internal standard of norketamine-d4 (100 µg/mL) were purchased from Cerilliant Co. (USA). High-performance liquid chromatography-grade ethyl acetate and methanol were obtained from Honeywell - Burdick & Jackson (USA), while analytical-grade formic acid was sourced from Fisher Scientific (USA). Sodium carbonate, sodium bicarbonate and sodium hydroxide were purchased from Katayama Chemical Industries Co. (Japan). Hydrochloric acid was acquired from Shimakyu's Pure Chemicals (Japan), and the derivatization reagent TFAA was obtained from Sigma-Aldrich Co. (USA). Sodium dihydrogen phosphate was sourced from PanReac AppliChem (Germany), and disodium hydrogen phosphate from J.T.Baker (USA). A 150-donor mixed-gender HLMs, nicotinamide adenine dinucleotide phosphate regenerating system solution A (NADPH A), and NADPH regenerating system solution B (NADPH B) were obtained from Corning (USA). Finally, four urine samples from individuals suspected of drug use were collected by the Taoyuan Police Department in Taiwan in accordance with Taiwanese legal regulations, with all personal identifiers removed.

Instrumentation

The GC-MS system comprised an Agilent 6890 GC coupled to an Agilent 5975 MSD, equipped with an Agilent 7683 Series autosampler. Chromatographic separation was achieved using an HP-5MS column (30 m × 0.25 mm i.d., 0.25 µm film thickness). The initial oven temperature was set at 80°C, ramped to 250°C at 15°C/min and held for 1 min, followed by a second ramp to 280°C at 30°C/min, held for 2 min, resulting in a total analysis time of 15.333 min. The injector temperature was maintained at 250°C, employing a splitless injection mode. High-purity helium (99.999%) served as the carrier gas at a constant flow rate of 1.0 mL/min. Electron impact ionization was performed with an ionization energy of 70 eV. The mass spectrometer operated in full scan mode, analyzing ions in the *m/z* ranges of 50–500.

For LC-QTOF-MS, methods similar to those in our previous study were adapted [19]. An Agilent 1260 LC system was coupled to an Agilent 6530B QTOF instrument. Chromatographic separation utilized a Poroshell 120 EC-C18 column (3.0 × 100 mm, 2.7 µm) maintained at 30°C. The mobile phases consisted of 0.1% formic acid in water (A) and 0.1% formic acid in methanol (B), with a gradient elution from 10% to 100% B over 10 min, a total run time of 18 min, a flow rate of 0.4 mL/min, and an injection volume of 5 µL.

Electrospray ionization (ESI) was conducted in positive ion mode using nitrogen as the drying gas (12 L/min at 350°C) and nebulizer gas (45 psi). Key parameters included a capillary voltage of 4000 V, skimmer voltage of 65 V, fragmentor voltage of 150 V, and octopole 1 RF voltage of 750 V. Data acquisition was performed in two modes: MS mode (*m/z* ranges: 100–1000, scan rate: 1 spectrum/s) and auto MS/MS mode (*m/z* ranges: 50–1000, scan rates of 3 spectra/s for MS and 2 spectra/s for MS/MS). Collision energies (CEs) were set at 10, 20, and 40 eV. The mass calibration procedure followed the protocol described in our previous study [19].

Pre-treatment of spiked and urine samples

The sample preparation was based on the method described by Lin et al. [20]. Standard solutions were spiked into 1 mL of blank urine, including the internal standard norketamine-d4 (200 ng/mL). Subsequently, 1 mL of Na_2CO_3/$NaHCO_3$ buffer (pH 10) and 3 mL of ethyl acetate were added, followed by vortexing for 10 min and centrifugation at 4,414 RCF for 5 min. The supernatant was transferred to a clean glass tube. The extraction was repeated with another 3 mL of ethyl acetate, and the combined supernatants were transferred to the same glass tube, followed by the addition of 10 µL of 1% HCl in methanol. The solvent was evaporated to near dryness in a 40°C water bath under a gentle stream of nitrogen gas. For urine samples, 1 mL of each sample was spiked with the internal standard and subjected to the same pre-treatment procedure. Finally, the extracts were

reconstituted in 200 μL of mobile phase A. Of this, 100 μL was for LC-QTOF-MS analysis, while the remaining 100 μL was evaporated to dryness, reconstituted in 50 μL of ethyl acetate, and derivatized with 50 μL of TFAA at 90°C for 20 min. After cooling to room temperature, the mixture was evaporated to dryness at 45°C under nitrogen and reconstituted in 100 μL of ethyl acetate for GC-MS analysis.

Acquisition of MS spectral data and model development

Mass spectra of each standard compound were acquired using Agilent Data Analysis software, with appropriate background subtraction. The spectra were converted into *m/z* and intensity data using the "Tabulate" function in the "Spectrum" module. Exported data were processed and focused on the *m/z* ranges of 50–318 (we use the code written by Python 3.9 ver.). Intensities were normalized to percentages, and each *m/z* value was treated as a feature. The *m/z* values within a 0.5 Da difference were grouped as a single *m/z* feature, and the intensity values of signals within this range were aligned and combined accordingly. This study followed the guideline of the Society of Toxicological and Forensic Chemistry (GTFCh) [21], which require that the complete mass spectrum includes all ions with relative intensities above 10%, such as molecular ions, adducts, characteristic fragments, and isotopic ions. Based on the guideline, all fragments with relative intensities above 10% were selected as model features, ensuring comprehensive spectral data.

Based on our previous study [22], feature extraction was conducted by using PCA. Two principal components were used as inputs for Logistic Regression (LR) classification. Model performance was visualized with a decision boundary plot, illustrating the theoretical ability to distinguish between classes. The training set consisted of 20 replicate spectra for each compound, prepared by mixing 200 ng of the standard with 50 μL of ethyl acetate and 50 μL of TFAA, followed by derivatization at 90°C for 20 min. After cooling to room temperature, the samples were evaporated to dryness at 45°C under nitrogen and reconstituted in 100 μL of ethyl acetate for GC-MS analysis. The test set included 20 replicate spectra for each compound, prepared by spiking standard solutions into blank urine. They were processed by the same pre-treatment procedure of urine samples. Model accuracy was used to evaluate performance. Finally, the mass spectral data of four urine samples were analyzedby the developed mass spectral model.

In vitro metabolism experiment

The *in vitro* metabolism experiment was conducted based on the methods described by Presley et al. [23, 24] and our previous study [19], with slight modifications. Each standard (1 mg/mL) was dried and reconstituted with deionized water to prepare a standard drug solution. Reaction mixtures were prepared by combining 1 μL of the drug standard, 138 μL of 100 mM phosphate buffer (Na_2HPO_4/NaH_2PO_4, pH 7.4) containing 10 mM $MgCl_2$, 5 μL of NADPH A, 1 μL of NADPH B, and 5 μL of pHLM, resulting in a total volume of 150 μL. The mixtures were thoroughly mixed and incubated at 37°C in a shaking incubator at 1,500 rpm for 7 h. After this, 100 μL of ice-cold acetonitrile was added to quench the reaction. The samples were then centrifuged at 21,379 × g at −4°C for 5 min. Finally, 150 μL of the supernatant was transferred to autosampler vials for LC-QTOF-MS analysis.

Identification of the in vitro and in vivo samples

Based on the studies by Gicquel et al. [18] and Joseph et al. [2], the potential metabolic pathways and metabolites of 2-FDCK include hydrogenation, *N*-demethylation, hydroxylation, deamination, dehydration, and oxidation. Initially, these potential metabolites were catalogued in the Personal Compound Database and Library (PCDL), including their compound names, molecular formulae, and accurate masses. Identification methods were adapted from our previous study [19, 22]. Qualitative analysis was performed using Agilent MassHunter Qualitative Analysis software (version B.07.00). The "Find Compounds by Formula" feature was used to confirm the formulae of the compounds listed in the PCDL. The qualitative criteria required a compound score of at least 60, based on the measured exact mass and isotope distribution compared with the proposed formula. The mass match tolerance was set at ±15 ppm. MS/MS spectra were extracted from the auto MS/MS mode for collision energies of 10, 20, and 40 eV, with a precursor tolerance of ±20 ppm. The major MS/MS fragments were compared with those reported in the literature [2, 18] to confirm metabolite identities. Once the *in vitro* metabolite results were

validated, the MS/MS spectra were integrated into the PCDL, enabling comparison with spectra obtained from urine samples for further confirmation of metabolites.

Results and discussion

Mass spectral data model development

The mass spectra of 2-FDCK-TFAA, 3-FDCK-TFAA and 4-FDCK-TFAA are shown in Fig. 1. Because most of the *m/z* values are highly similar, it is challenging to differentiate or classify these compounds solely based on mass spectral data or similarity scores. Sixty training spectra (20 for each class) were processed. Only *m/z* values with relative intensities exceeding 10% were retained. We remove those *m/z* values that did not be included in all training spectrum. The left 21 *m/z* values are 69, 95, 101, 109, 110, 121, 133, 135, 136, 146, 147, 162, 163, 164, 192, 220, 246, 260, 273, 289 and 317.

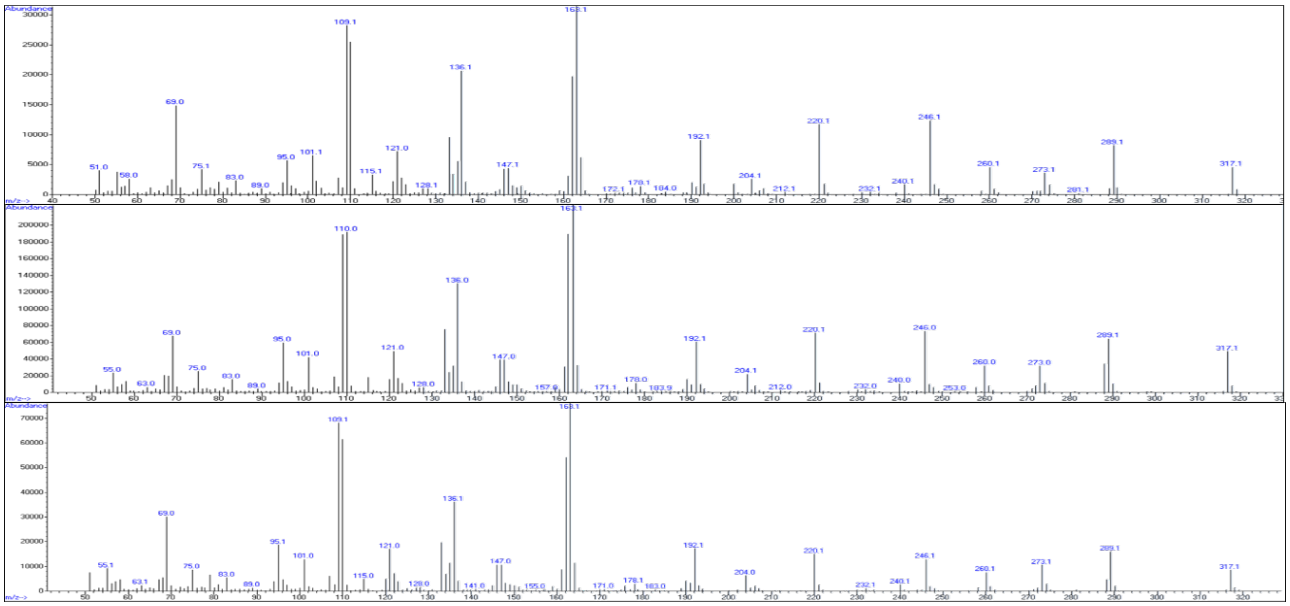

Fig. 1. Mass spectra of 2-FDCK-TFAA, 3-FDCK-TFAA, and 4-FDCK-TFAA.

With PCA and LR, we develop a mass spectral classification model base on the left *m/z* values and their corresponding relative intensities. The resulting mass spectral model is shown in Fig. 2. The decision boundaries established by LR clearly separate 2- FDCK, 3- FDCK and 4-FDCK into three distinct classes. The contribution rates of each m/z value to PC1 and PC2 are illustrated in Fig. 3. Notably, fragments with higher contributions were *m/z* 162, 246, 136 and 220, and their fragment structures for 2-FDCK-TFAA are summarized in Table 1. Fig. 4 presents a box plot analysis of the relative intensity distributions for the most significant m/z values across the three classes. It illustrates their intensity ranges and inter-class differences, which highlight their utility in distinguishing 2-FDCK, 3-FDCK and 4-FDCK.

To validate the model, a total of 60 test spectra (20 for each class) were analyzed. The classification results are displayed in the scatter plot in Fig. 5. The model achieves 100% accuracy and effectively classifies all test spectra into three distinct categories. We demonstrate its reliability in accurately distinguishing 2-FDCK, 3-FDCK and 4-FDCK.

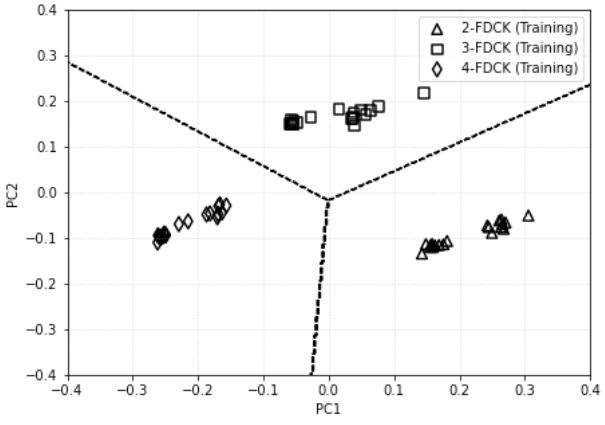

Fig. 2. Mass spectral classification model using PCA and LR.

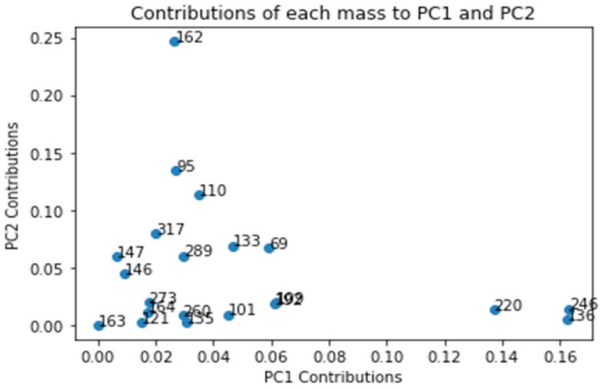

Fig. 3. Contribution of each *m/z* value to PC1 and PC2.

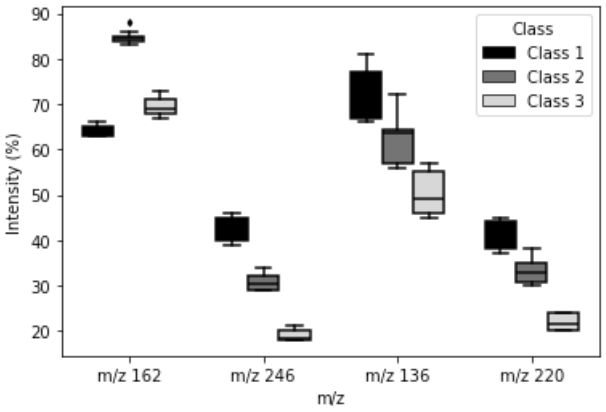

Fig. 4. Relative intensity ranges of the four most intense *m/z* peaks across the different categories, represented as a box plot.

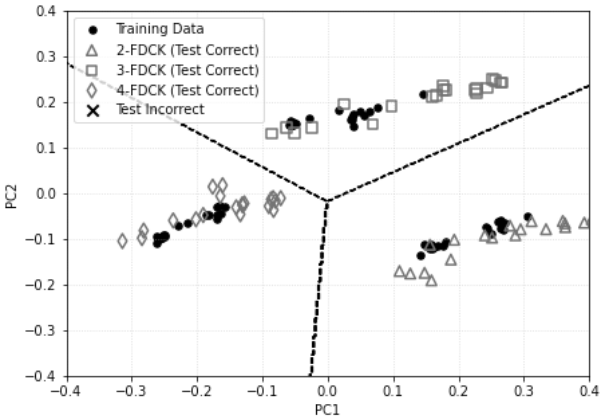

Fig. 5. Classification results of the test set using the mass spectral model, demonstrating correct classification.

Table 1. Fragment structures of *m/z* 162, 246, 136, and 220, represented using 2-FDCK-TFAA.

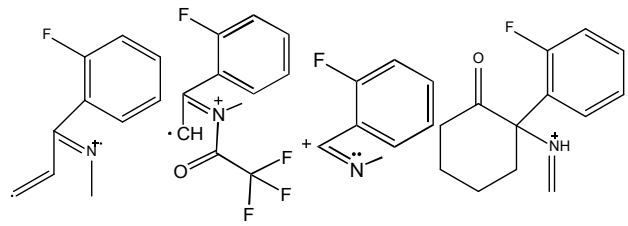

m/z 162	m/z 246	m/z 136	m/z 220

Application of Model to urine sample classification

Four urine samples are classified by the established model. Fig. 6 shows the predicted results. Each sample is classified as 2-FDCK. During the analysis of urine sample spectra, it was noted that low-concentration samples are susceptible to background interference. Moreover, spectral background subtraction can exaggerate variations in fragment intensities. Thus, careful inspection of the original mass spectra and appropriate background subtraction are crucial prior to classification. For samples with extremely low concentrations or excessive interference, the model may not be suitable for classification. In this study, a mass spectral model for 2-FDCK-TFAA, 3- FDCK-TFAA and 4-FDCK-TFAA was developed. The derivatization step generated more abundant fragment ions, facilitating subsequent classification of urine samples. This approach offers potential for the differentiation of structurally similar substances in forensic and analytical applications.

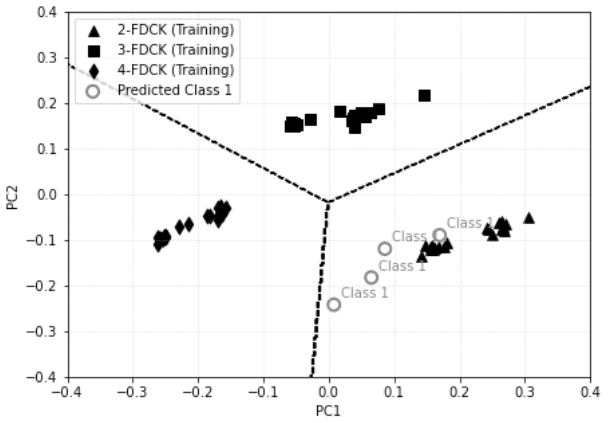

Fig. 6. Classification results of four urine samples using the established mass spectral model, all identified as 2-FDCK.

In vitro metabolism of 2-FDCK, 3-FDCK and 4-FDCK

After a 7-hour incubation, the *in vitro* metabolism results, RT, and mass deviations of 2-FDCK, 3-FDCK and 4-FDCK are summarized in Table 2. Hydroxy-2-FDCK exhibited three peaks (M2(a), M2(b), and M2(c)), while dihydro-2-FDCK (M8(a), M8(b)), dihydro-nor-2-FDCK (M9(a), M9(b)), and dihydro-deamino-nor-2-FDCK (M11(a), M11(b), M11(c)) each displays two or three peaks, respectively. All peaks within the same metabolite category share identical MS/MS spectra, differing only in fragment intensity, likely due to variations in the hydroxylation position on the benzene ring, though their exact locations remain undetermined. A total of 17 Phase I metabolites are identified, involving metabolic reactions such as hydrogenation, *N*-demethylation, hydroxylation, deamination and dehydration, as illustrated in Fig. 7 using 2-FDCK as an example. The precursor ion mass deviations range from -2.86 to 4.09 ppm, and the full MS/MS spectra exhibit characteristic fragment ions consistent with those reported by Gicquel et al. [18] Furthermore, no defluorinated metabolites, such as DCK, are detected, aligning with the findings of Joseph et al. [2] in their HLMs study.

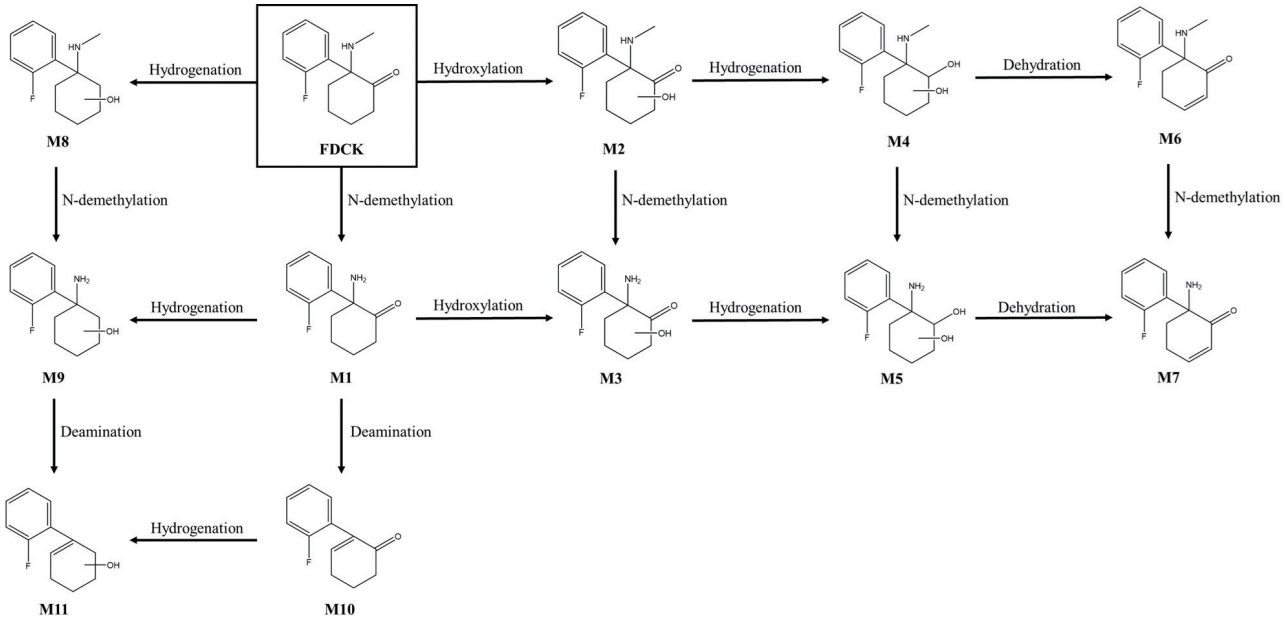

Fig. 7. Identification of Phase I metabolites and their metabolic pathways (2-FDCK as an example), including hydrogenation, N-demethylation, hydroxylation, deamination, and dehydration.

Table 2. *In vitro* metabolism results of 2-FDCK, 3-FDCK and 4-FDCK.

				2-FDCK			3-FDCK			4-FDCK		
NPS and Metabolites		Formula	Monoiso-topic mass	RT[a]	Measure of $[M+H]^+$	Mass error (ppm)	RT[a]	Measure of $[M+H]^+$	Mass error (ppm)	RT[a]	Measure of $[M+H]^+$	Mass error (ppm)
Parent	FDCK	$C_{13}H_{16}FNO$	222.1289	6.06	222.1289	0.00	6.26	222.1289	0.00	6.37	222.1290	0.45
M1	Nor-FDCK	$C_{12}H_{14}FNO$	208.1132	6.00	208.1132	0.00	6.34	208.1133	0.48	6.45	208.1133	0.48
M2(a)	Hydroxy-FDCK	$C_{13}H_{16}FNO_2$	238.1238	3.42	238.1237	-0.42	4.54	238.1235	-1.26	4.72	238.1235	-1.26
M2(b)	Hydroxy-FDCK	$C_{13}H_{16}FNO_2$	238.1238	4.47	238.1237	-0.42	4.84	238.1247	3.78	5.02	238.1234	-1.68
M2(c)	Hydroxy-FDCK	$C_{13}H_{16}FNO_2$	238.1238	8.34	238.1233	-2.10	-	-	-	8.17	238.1236	-0.84
M3	Hydroxy-nor-FDCK	$C_{12}H_{14}FNO_2$	224.1081	7.30	224.1090	4.02	-	-	-	-	-	-

NPS and Metabolites		Formula	Monoisotopic mass	2-FDCK			3-FDCK			4-FDCK		
				RT[a]	Measure of $[M+H]^+$	Mass error (ppm)	RT[a]	Measure of $[M+H]^+$	Mass error (ppm)	RT[a]	Measure of $[M+H]^+$	Mass error (ppm)
M4	Hydroxy-hydro-FDCK	$C_{13}H_{18}FNO_2$	240.1394	5.12	240.1403	3.75	5.69	240.1393	-0.42	5.82	240.1389	-2.08
M5	Dihydro-hydroxy-nor-FDCK	$C_{12}H_{16}FNO_2$	226.1238	4.68	226.1236	-0.88	5.35	226.1235	-1.33	-	-	-
M6	Dehydro-FDCK	$C_{13}H_{14}FNO$	220.1132	5.60	220.1128	-1.82	5.78	220.1135	1.36	5.88	220.1141	4.09
M7	Dehydro-nor-FDCK	$C_{12}H_{12}FNO$	206.0976	5.20	206.0977	0.49	5.68	206.0974	-0.97	5.80	206.0980	1.94
M8(a)	Dihydro-FDCK	$C_{13}H_{18}FNO$	224.1445	6.22	224.1446	0.45	7.17	224.1446	0.45	7.29	224.1445	0.00
M8(b)	Dihydro-FDCK	$C_{13}H_{18}FNO$	224.1445	7.07	224.1441	-1.78	7.42	224.1441	-1.78	7.52	224.1442	-1.34
M9(a)	Dihydro-nor-FDCK	$C_{12}H_{16}FNO$	210.1289	5.93	210.1283	-2.86	6.78	210.1289	0.00	-	-	-
M9(b)	Dihydro-nor-FDCK	$C_{12}H_{16}FNO$	210.1289	6.54	210.1284	-2.38	6.99	210.1287	-0.95	-	-	-
M10	Deamino-nor-FDCK	$C_{12}H_{11}FO$	191.0867	5.99	191.0865	-1.05	6.34	191.0866	-0.52	6.45	191.0866	-0.52
M11(a)	Dihydro-deamino-nor-FDCK	$C_{12}H_{13}FO$	193.1023	5.93	193.1020	-1.55	7.00	193.1022	-0.52	7.11	193.1022	-0.52
M11(b)	Dihydro-deamino-nor-FDCK	$C_{12}H_{13}FO$	193.1023	6.21	193.1022	-0.52	7.17	193.1021	-1.04	7.28	193.1022	-0.52
M11(c)	Dihydro-deamino-nor-FDCK	$C_{12}H_{13}FO$	193.1023	7.07	193.1023	0.00	-	-	-	-	-	-

[a] RT: retention time.
-Non-detected

Notably, M11(a) and M9(a) share the same RT, with M9(a) producing an m/z 193.1023 fragment in its MS/MS spectrum—corresponding to the exact mass of M11(a). This suggests the occurrence of in-source fragmentation (ISF) during the electrospray ionization (ESI) process [25]. A similar pattern is observed for M9(b) and M11(c), where identical RT is noted. To prevent misidentification, M11(a) and M11(c) are excluded from further analysis. Conversely, M11(b) did not exhibit RT overlap with other dihydro-nor-FDCK isomers, indicating it is an actual metabolite rather than an ISF artifact.

A comparative analysis of RT revealed that the differences between 2-FDCK and 3-FDCK metabolites are more pronounced (≥0.181 min), while the RT differences between 3-FDCK and 4-FDCK metabolites are relatively smaller (≥0.103 min). This suggests that RT can serve as a distinguishing factor between 2-FDCK and the other two isomers, 3-FDCK and 4-FDCK.

The relative proportions of 2-FDCK, 3-FDCK, 4-FDCK and their metabolites, expressed as the ratio of individual peak areas to the sum of the peak areas of the parent compound and all detected metabolites (100%), are summarized in Fig. 8. In the case of 2-FDCK, a total of 15 metabolites are identified, with the unmetabolized parent compound accounting for approximately 30% of the total peak area. The predominant metabolite is nor-2FDCK (M1), a product of N-demethylation, comprising 30%. The secondary metabolite is M8(a), formed via hydrogenation, with a relative proportion of 14%.

For 3-FDCK, 13 metabolites are detected, with the parent compound constituting 20%. The most abundant metabolite was M8(a) (38%), followed by M1 (19%). Similarly, 4-FDCK yield 11 detected metabolites, with the unmetabolized parent compound comprising a relatively higher proportion of 48%. The predominant metabolite is M8(a) (18%), while M1 (13%) is the second most abundant.

The *in vitro* metabolism results indicate that 3-FDCK undergoes the fastest metabolism among the three isomers. Furthermore, the third most abundant metabolite varied among the isomers. For 2-FDCK, the third most abundant metabolite is M2(a), formed via hydroxylation. For 3-FDCK, it is M8(b), another

hydrogenated product similar to M8(a). For 4-FDCK, it is deamino-4FDCK (M10), formed via deamination from M1. Interestingly, M9(a) and M9(b), hydrogenated product of M1, are not detected in 4-FDCK, possibly due to its low concentration. This suggests that, in addition to differences in metabolic rates, positional isomers (*ortho-, meta-* and *para*-substituted FDCK) exhibit distinct metabolite distributions and relative proportions.

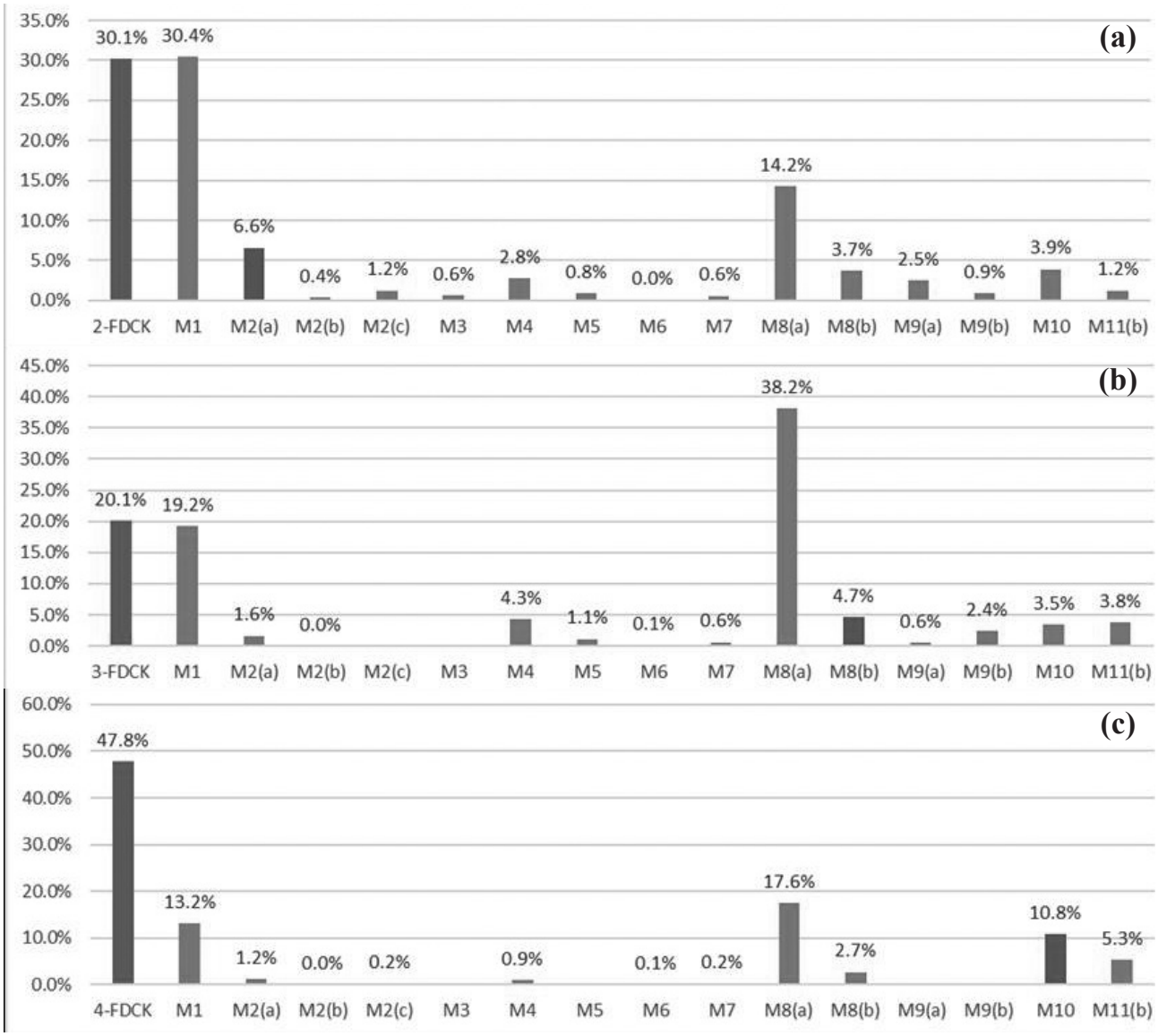

Fig. 8. Relative proportions of 2-FDCK (a), 3-FDCK (b), 4-FDCK(c) and their metabolites, expressed as the ratio of individual peak areas to the total peak area (100%).

Analysis of urine samples in relation to the in vitro metabolism results

The pretreatment method for 2-FDCK was first validated before being applied to the analysis of four urine samples, which had been previously confirmed as 2-FDCK using the developed classification model. The detected metabolites in these urine samples were identified by comparing their RT and MS/MS spectra with those of the 15 Phase I metabolites observed in the *in vitro* metabolism study. The ratios of individual peak areas of 2-FDCK and its metabolites to the total peak area of the parent compound and all detected metabolites (100%) are summarized in Fig. 9.

Among the real samples, Real 1 exhibit a higher proportion of the unmetabolized parent compound, with M9(a) and M9(b) as the primary metabolites. In contrast, Real 2 and Real 3 are predominantly metabolized into M1 and M8(a), consistent with the major metabolites

observed in the *in vitro* study. Notably, Real 4 contain only 1% of the parent compound, with M9(a) and M9(b) as the primary metabolites. Additionally, dihydro-hydroxy-nor-2FDCK (M5) is detected at a relatively high proportion, suggesting that Real 4 may represent a later stage of metabolism, where multiple metabolic transformations had already occurred. Due to individual differences in metabolic rate, drug dosage, and time of administration, the metabolite distribution alone is insufficient to distinguish between 2-FDCK, 3-FDCK and 4-FDCK. However, by integrating the RT and MS/MS spectral comparison of the parent compound and its metabolites, the findings confirm that all four urine samples contain 2-FDCK rather than 3-FDCK or 4-FDCK.

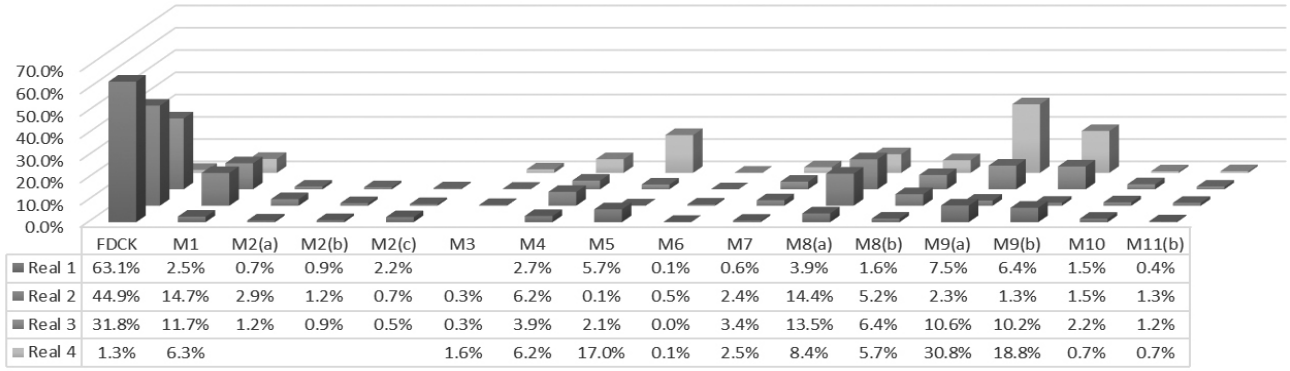

	FDCK	M1	M2(a)	M2(b)	M2(c)	M3	M4	M5	M6	M7	M8(a)	M8(b)	M9(a)	M9(b)	M10	M11(b)
Real 1	63.1%	2.5%	0.7%	0.9%	2.2%		2.7%	5.7%	0.1%	0.6%	3.9%	1.6%	7.5%	6.4%	1.5%	0.4%
Real 2	44.9%	14.7%	2.9%	1.2%	0.7%	0.3%	6.2%	0.1%	0.5%	2.4%	14.4%	5.2%	2.3%	1.3%	1.5%	1.3%
Real 3	31.8%	11.7%	1.2%	0.9%	0.5%	0.3%	3.9%	2.1%	0.0%	3.4%	13.5%	6.4%	10.6%	10.2%	2.2%	1.2%
Real 4	1.3%	6.3%				1.6%	6.2%	17.0%	0.1%	2.5%	8.4%	5.7%	30.8%	18.8%	0.7%	0.7%

Fig. 9. Analysis of 2-FDCK and its metabolites in four urine samples.

A comparison with existing literature reveals that Mestria et al. [17] identified M1, M8, and M9 as the predominant metabolites in their study on blood and hair samples. Similarly, Gicquel et al. [18] reported concordant findings in *in vitro* liver microsome and hepatocyte studies, as well as in blood, urine, and bile samples, and recommended M1 and M8 as primary analytical targets. In contrast, Joseph et al. [2], based on their study involving HLM and various biological matrices, including blood and hair, proposed M7 as a key biomarker for hair analysis and M5 for urine detection. Additionally, their HLM study identified M1 as the most abundant metabolite, followed by deamino-nor-2FDCK (M10). The findings from the present *in vitro* metabolism study exhibit greater concordance with those of Gicquel et al. [18], reinforcing the suitability of M1 and M8 as primary metabolic markers. Furthermore, analysis of urine specimens supports M9(a) and M9(b) as additional viable detection targets. Notably, in Real 4, M5 was detected at a relatively high abundance, aligning with Joseph et al.'s [2] recommendation for urinary biomonitoring. The identification of these metabolites as analytical markers is particularly advantageous for extending the detection window, especially in cases where 2-FDCK concentrations are low, thereby enhancing the reliability of forensic and toxicological assessments.

A comparative evaluation of 2-FDCK and ketamine metabolism reveals distinct enzymatic pathways. Ketamine undergoes *N*-demethylation primarily mediated by CYP3A4 and CYP2B6, yielding norketamine, which is subsequently metabolized by CYP2A6 and CYP2B6 to form hydroxynorketamine and dehydronorketamine [26]. While 2-FDCK follows an analogous *N*-demethylation pathway, its subsequent metabolic diverges, primarily undergoing hydrogenation, with hydroxylated (M3) and dehydrogenated (M7) metabolites detected at relatively low levels. It is important to note that the *in vitro* metabolism methodology and urinary sample extraction protocol employed in this study were not optimized for the detection of Phase II metabolites. Future studies will address this limitation by incorporating methods for a more comprehensive characterization of 2-FDCK metabolism.

Conclusion

This study successfully develops a mass spectral classification model by reference standards to differentiate 2-FDCK, 3-FDCK and 4-FDCK. The

model achieves 100% accuracy in classifying the test set and is further applied to urine samples, confirming that all specimens contained 2-FDCK. These findings demonstrate the model's effectiveness in distinguishing between 2-FDCK, 3-FDCK and 4-FDCK with high reliability. In addition, an *in vitro* metabolism study using HLMs is conducted to characterize the metabolic pathways of 2-FDCK, 3-FDCK and 4-FDCK. While the availability of metabolite reference standards remains limited, *in vitro* metabolism studies provide a valuable approach for predicting metabolite profiles of emerging substances and establishing spectral databases. The results reveals differences in metabolic rates and metabolite distribution among the three isomers. By comparing *in vitro* metabolism data with urine samples, the pre-established spectral database facilitates rapid identification of metabolites. Although the major metabolites are not entirely identical between *in vitro* and in vivo samples, nor-2-FDCK (M1), dihydro-2-FDCK (M8(a)), and dihydro-nor-2-FDCK (M9(a), M9(b)) are identified as key biomarkers for 2-FDCK detection. These metabolites can serve as alternative targets when the parent compound is present at low concentrations, thereby improving detection sensitivity. Overall, this study demonstrates the applicability of mass spectral modeling in differentiating positional isomers of FDCK and highlights their distinct metabolic profiles *in vitro*. The proposed approach provides a valuable reference for forensic and toxicological analysis, offering a potential solution for the differentiation of structurally similar positional isomers.

Acknowledgements

This study was supported by the Ministry of the Interior of Taiwan (ROC) [grant numbers 112-0805-02-28-01, 2023; 113-0805-02-28-01, 2024].

References

1. Dimitrov I, Denny WA, Jose J. Syntheses of ketamine and related analogues: a mini review. Synthesis 2018; 50:4201-15.
2. Joseph D, Lesueur C, Zerizer F, Fenot A, Alvarez JC, et al. Characterization of extensive 2-fluorodeschloroketamine metabolism in pooled human liver microsomes, urine and hair from an addicted patient using high-resolution accurate mass spectrometry. J Anal Toxicol 2023; 47(6):504-16.
3. Luo X, Zhang D, Zhang F, Luo Q, Huang K, et al. Comparative analysis and structure identification of oxidative metabolites and hydrogenation metabolite enantiomers for 2-fluorodeschloroketamine. J Anal Toxicol 2023; 47(5):436-47.
4. Tang MHY, Li TC, Lai CK, Chong YK, Ching CK, et al. Emergence of new psychoactive substance 2-fluorodeschloroketamine: toxicology and urinary analysis in a cluster of patients exposed to ketamine and multiple analogues. Forensic Sci Int 2020; 312:110327.
5. Gao J, Xu B, Yang R, Zhang H. Screening strategy for ketamine-based new psychoactive substances using fragmentation characteristics from high resolution mass spectrometry. Forensic Sci Int 2023; 347:111677.
6. Li F, Qiao Y, Chen Y, Li N, Yang M, et al. N-ethylnorketamine has anesthetic and analgesic effects with abuse liability. Behav Brain Res 2022; 435:114052.
7. Roth BL, Gibbons S, Arunotayanun W, Huang XP, Setola V, et al. Correction: the ketamine analogue methoxetamine and 3- and 4-methoxy analogues of phencyclidine are high affinity and selective ligands for the glutamate NMDA receptor. PLoS One 2018; 13(3):e0194984.
8. Sassano-Higgins S, Baron D, Juarez G, Esmaili N, Gold M. A review of ketamine abuse and diversion. Depress Anxiety 2016; 33(8):718-27.
9. Taiwan Ministry of Health and Welfare. List of new psychoactive substances (NPS) detected in Taiwan. Available at: https://www.fda.gov.tw/tc/site.aspx?sid=9958 (accessed 30 January 2025).
10. Chhabra N, Aseri ML, Padmanabhan D. A review of drug isomerism and its significance. Int J Appl Basic Med Res 2013; 3(1):16-8.
11. Verhoeven M, Bonetti JL, Kranenburg R, Asten AV. Chemical identification and differentiation of positional isomers of novel psychoactive substances: a comprehensive review. TrAC Trends Anal Chem 2023; 166:117157.
12. Bonetti JL, Samanipour S, van Asten AV. Utilization of machine learning for the differentiation of positional NPS isomers with direct analysis in

real time mass spectrometry. Anal Chem 2022; 94(12):5029-40.
13. Kranenburg RF, Peroni D, Affourtit S, Westerhuis JA, Smilde AK, et al. Revealing hidden information in GC-MS spectra from isomeric drugs: chemometrics based identification from 15 eV and 70 eV EI mass spectra. Forensic Chem 2020; 18:100225.
14. Bonetti J. Mass spectral differentiation of positional isomers using multivariate statistics. Forensic Chem 2018; 9:50-61.
15. Chikumoto T, Kadomura N, Matsuhisa T, Kawashima H, Kohyama E, et al. Differentiation of FUB-JWH-018 positional isomers by electrospray ionization-triple quadrupole mass spectrometry. Forensic Chem 2019; 13:100157.
16. Kranenburg RF, Verduin J, Stuyver LI, Ridder RD, Beek AV, et al. Benefits of derivatization in GC-MS-based identification of new psychoactive substances. Forensic Chem 2020; 20:100273.
17. Mestria S, Odoardi S, Biosa G, Valentini V, Masi GD, et al. Method development for the identification of methoxpropamine, 2-fluoro-deschloroketamine and deschloroketamine and their main metabolites in blood and hair and forensic application. Forensic Sci Int 2021; 323:110817.
18. Gicquel T, Pelletier R, Richeval C, Gish A, Hakim F, et al. Metabolite elucidation of 2-fluoro-deschloroketamine (2F-DCK) using molecular networking across three complementary in vitro and in vivo models. Drug Test Anal 2022; 14(1):144-53.
19. Yeh Y-L, Wang S-M. Quantitative determination and metabolic profiling of synthetic cathinone eutylone in vitro and in urine samples by liquid chromatography tandem quadrupole time-of-flight mass spectrometry. Drug Test Anal 2022; 14(7):1325-37.
20. Lin H-R, Lua A-C. Simultaneous determination of amphetamines and ketamines in urine by gas chromatography/mass spectrometry. Rapid Commun Mass Spectrom 2006; 20(11):1724-30.
21. Scientific Committee Quality Control, GTFCh. Guideline for quality control in forensic-toxicological analyses. 2018. Available at: https://www.gtfch.org/cms/images/stories/files/Guidelines-for-quality-control-in-forensic-toxicological-analyses-GTFCh-20090601-20180125.pdf (accessed 30 January 2025).
22. Yeh Y-L, Wen C-Y, Hsieh C-L, Chang Y-H, Wang S-M. In vitro metabolic studies and machine learning analysis of mass spectrometry data: a dual strategy for differentiating alpha-pyrrolidinohexiophenone (alpha-PHP) and alpha-pyrrolidinoisohexanophenone (alpha-PiHP) in urine analysis. Forensic Sci Int 2024; 361:112134.
23. Presley BC, Logan BK, Jansen-Varnum SA. Phase I metabolism of synthetic cannabinoid receptor agonist PX-1 (5F-APP-PICA) via incubation with human liver microsomes and UHPLC-HRMS. Biomed Chromatogr 2020; 34(3):e4786.
24. Presley BC, Logan BK, Jansen-Varnum SA. In vitro metabolic profile elucidation of synthetic cannabinoid APP-CHMINACA (PX-3). J Anal Toxicol 2020; 44(3):226-36.
25. Guo J, Shen S, Xing S, Yu H, Huan T. ISFrag: de novo recognition of in-source fragments for liquid chromatography-mass spectrometry data. Anal Chem 2021; 93(29):10243-50.
26. Zanos P, Moaddel R, Morris PJ, Riggs LM, Highland JN, et al. Ketamine and ketamine metabolite pharmacology: insights into therapeutic mechanisms. Pharmacol Rev 2018; 70(3):621-60.